Reliability of portable X-ray Fluorescence for the chemical characterisation of ancient corroded copper-tin alloys

Reliability of portable X-ray Fluorescence for the chemical characterisation of ancient corroded copper tin alloys

Simone Robotti [a,b], Paola Rizzi [a], Chiara Soffritti [b], Gian Luca Garagnani [b], Christian Greco [c], Federica Facchetti [c], Matilde Borla [d], Lorenza Operti [a,e], Angelo Agostino [a,e],

[a] Dipartimento di Chimica, Università di Torino, Via Giuria 7, 10125 Torino, Italy
[b] Dipartimento di Ingegneria, Università di Ferrara, Via Saragat 1,44122 Ferrara, Italy
[c] Fondazione Museo delle Antichità Egizie di Torino, Via Accademia delle Scienze, 6, 10123 Torino, Italy
[d] Soprintendenza Archeologia, Belle Arti e Paesaggio per la città metropolitana di Torino, Piazza San Giovanni, 2, 10122 Torino, Italy
[e] CRISDI (Interdepartmental Centre for Crystallography), Via Giuria 7, Torino, Italy

Abstract

This paper examines the effect of different corrosion patinas on the chemical composition of copper tin alloys de-tected by portable X-ray Fluorescence Spectroscopy (pXRF). Specimens of $Cu_{88}Sn_{12}$ alloy with a composition close to that of ancient Egyptian copper-based alloys were corroded in three different aqueous solutions contain-ing aggressive anions that can be found in Egyptian soil, for a maximum time of three months. After each sample was extracted, the elemental composition was determined with pXRF and the surface morphology and cross-sec-tions were observed by metallographic microscopy to measure the thickness of the corrosion patinas. The cross-section of selected samples was analysed with Scanning Electron Microscopy equipped with Energy Dispersive X-ray Spectrometer (SEM-EDS). During the corrosion evolution of the copper alloy in the corrosive solutions of chlorides, decuprification phenomena made XRF data less accurate due to the development and thickening of Sn compounds (oxides or chlorides). Another problem encountered in the detection of the chemical composition of the $Cu_{88}Sn_{12}$ alloy was the bronze disease that strongly increased the corrosion process leading to the forma-tion of an outer layer of atacamite and paratacamite, reaching a thickness of 150 μm. Conversely, during the cor-rosion process of the samples immersed in a sulphate solution, no changes in the initial composition of the $Cu_{88}Sn_{12}$ alloy were observed. The attenuation effect of the Sn concentration, by the thickness of green/dark green patinas with a high chloride content was observed on two Egyptian toilet spoons from the Museo Egizio (Turin) using pXRF. Following comparison of the chemical compositions in different corrosion patinas, it emerged that the red and grey patinas did not suffer the attenuation effects and, at these points of analysis, a re-liable chemical characterisation of the alloy was obtained.

1. Introduction

Due to different possible interactions between ancient metallic arte-facts and various environments, as well as the different preservation conditions, the corrosion processes of metallic materials remain a com-plex topic that is still under investigation. Moreover, the use of portable X-ray Fluorescence (pXRF) devices to measure the elemental composi-tion of bulk and corrosion layers of copper alloys [1–7], brings into ques-tion the reliability of the composition determined on metallic materials sometimes covered with thick patina layers, the composition of which can differ from the original composition of the alloy. Therefore, even though XRF Spectroscopy has the potential to provide precise and fast results, allowing for non-destructive measurements of archaeological applications to be made in situ [8], it is important to experimentally de-termine in which conditions corrosion layers can affect the elemental results in order to enable the measurements of reliable compositions.

Ancient bronze artefacts are subjected to corrosion processes that can involve the formation of corrosion patinas on their surface, besides possible inter-granular or intra-granular corrosion processes or galvanic electrochemical processes [9–11]. The corrosion processes of archaeo-logical bronze were described by Robbiola et al. and classified as two types. In the type I corrosion process (or on “even” surfaces), the inter-action of the artefacts with the soil leads to a galvanic corrosion with a selective dissolution of copper (i.e. decuprification) from the alloy and the consequent oxidation of the tin enriched layer with the formation of an outer Sn oxide rich layer, superimposed onto an internal layer composed of oxides and hydroxides in which the amount of Cu in-creases with respect to the outer layer. The type II corrosion process is due to a high dissolution rate of the alloy that involves the formation of three corrosion layers: (1) an outer zone of green Cu(II) compounds as malachite; (2) an intermediate red layer of cuprous oxide, often fragmented; (3) an internal layer characterised by high tin contents due to selective Cu dissolution associated with soil elements, O and Cl [12]. A recent study of the degradation phenomena of a bronze bowl of the Achaemenid Empire (559–330 BCE) containing about 11% tin was analysed by pXRF, Raman spectroscopy and scanning electron microscopy equipped with energy dispersive spectroscopy (SEM-EDS). The results showed new corrosion structures: (1) a copper oxide (cuprite, tenorite)/tin oxide (cassiterite) layer; (2) a copper hydroxycarbonate (malachite, azurite) layer; (3) a copper (II) basic carbonate top layer, merged with other soil components [13].

The aim of this work is to study the corrosion process of a $Cu_{88}Sn_{12}$ alloy in different conditions in order to determine the corrosion prod-ucts and to test the applicability of the pXRF when determining the chemical composition of the $Cu_{88}Sn_{12}$ alloy at different degrees of corro-sion. Furthermore, the applicability of the method is proposed for the chemical characterisation of two toilet spoon copper based alloys C.6428 and P.624 from the Museo Egizio (Turin).

The $Cu_{88}Sn_{12}$ alloy was chosen due to its similar composition to the Egyptian bronzes of the New Kingdom (1550–1069 BCE). The use of copper alloys started in Egypt from the middle Predynastic period [14,15]. From numerous analyses [16–24] it was concluded that arseni-cal copper alloys were used with an As content between 1 and 8% and Sn as a trace element (b1%) in the Old Kingdom (2700–2200 BCE) and Middle Kingdom (1990–1630 BCE). Bronze was used in the New Kingdom, where Sn usually varied between 2 and 16% [25]. During the Late Period, Ptolemaic and Roman Period, the Sn concentrations can exceed 20% [26].

This study aims to be a preliminary research in the systematic anal-ysis of the frameworks of ancient copper alloys.

2. Materials and methods

$Cu_{88}Sn_{12}$ alloy was produced by casting the master alloy into three bar ingots and 28 samples (dimensions 2 × 2 × 1 cm) were obtained.

In order to perform the corrosion tests, three solutions were selected from the literature containing aggressive anions compatible with those obtained from the analysis carried out on Egyptian soils [27–30]. The so-lutions contained: 15.07 g of $(NH_4)_2CO_3$ and 10.02 g of NH_4Cl in 100 mL of de-ionised water (solution A); 0.6 g of $KClO_3$, 0.3 g of $CuSO_4 \cdot 5\ H_2O$ and 0.4 g of $N_2SO_4 \cdot 10\ H_2O$ in 100 mL of de-ionised water adjusted to pH = 3 with H_2SO_4 (solution B); 10.02 g of $Cu(NO_3)_2 \cdot 3\ H_2O$ and 10.01 g of NaCl in 100 mL of de-ionised water (solution C).

The corrosion tests were conducted through immersion at room temperature in order to prevent evaporation of the solutions for differ-ent degrees of corrosion corresponding to predetermined times in the solutions (0, 1, 3, 7, 10, 15, 30, 60, 90 days (d)).

Each sample, previously grounded by abrasive silicon carbide papers of grade 180, 500, 1000, 2500, respectively, and then polished with dia-mond paste from 6 to 3 μm, were immersed in solutions in glass beakers closed with parafilm for 15 days, while the specimens from 30 days to 90 days were immersed in solutions in polyethylene bottles to avoid evaporation of the solution.

The specimens were removed from the solutions, rinsed with de-ionised water and left to dry. Subsequently, the $Cu_{88}Sn_{12}$ samples were observed with an optical microscope and were analysed by X-ray Fluorescence (XRF), X-ray diffraction (XRD) and Scanning Elec-tron microscopy (SEM). All XRF analyses were carried out by a Thermo Niton™ (USA) XL3t-900 EDXRF spectrometer, equipped with a silver target and a large-area silicon drift detector (SDD), with an energy res-olution of 136 eV, calculated at 5.9 keV. The geometry used was 30°/30°, with a working distance of 2 mm orthogonal to the detector/source plane. The total analysis time was 120 s or 240 s, subdivided into four fractions (to optimise different energy ranges) respectively of 30 s or 60 s each for the "Patina" algorithm, and 60 s or 120 s subdivided into two fractions respectively of 30 s or 60 s each for the "Metals" algorithm. The different ranges were 50 keV at 50 μA with a Mo filter, 40 keV at 50 μA with a Fe/Al filter, 20 keV at 95 μA with a Cu filter and 8 keV at 95 μA with no filter, for the "Patina" method and 40 keV at 50 μA with a Fe/Al filter, 15 keV at 95 μA with a Fe filter and 6 keV at 95 μA for the "Metals" method. The spectra were processed using home-made software and the results were compared with the WinAxil CAN-BERRA commercial software. The instrument was kept in position by a custom stage allowing micrometric movements and all measurements to be conducted in air with a small spot (3 mm diameter). The "Patina" algorithm made it possible to detect the alloy and light elements (Cl, S, Si, Ca, K, Al, P), i.e. the chemical elements of the soil and corrosion products, while the "Metals" algorithm made it possible to detect only the elements present in the bulk. "Dark Matrix" (DM) is the concentra-tion of the elements set that were not detected by XRF spectrometer (e.g. H, O, Na etc.).

The difference between "metal" and "patina" methods can be summarized on the difference between algorithms in considering the

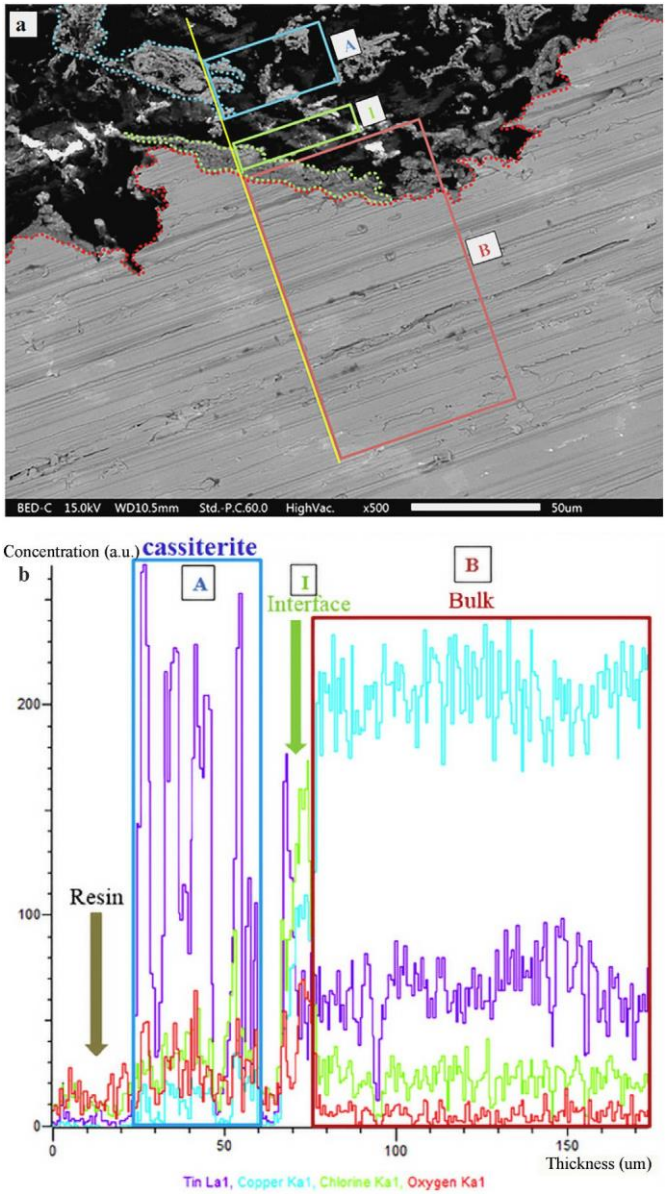

Fig. 1. SEM micrograph (a) and EDS line mapping (b) of the sample A_90d with the indication of patinas evolution.

scattering curves (elastic and inelastic) in the quantification of the dark matrix. In the case of "patina" algorithm, we define the contribution of light elements in the variation of the metal alloy composition including the not measurable elements recoiled in the dark matrix. In the "metal" algorithm approach, instead, just the metal elements are quantified and all the results are normalized.

In order to validate the quantitative analyses, measurements were conducted on certified composition standards. The Certified Standard Reference Materials (CRM): 31XB22E, 31XB17E, 31XMNB4E, 33XGM8F, 32XALB4G and 55XG900J3F, were produced by MBH Ltd. Each standard was analysed with both of the two quantitative algorithms and with different measurement times: 60 s (30 s for each energy range), 120 s (60 s for each energy range) and 180 s (90 s for each energy range) for the "Metals" algorithm; 12 0 s (30 s for each en-ergy range) and 240 s (60 s for each energy range) for the "Patina" algorithm.

The $Cu_{88}Sn_{12}$ alloy composition was calculated by the arithmetic mean of all the measurements carried out with the "Metals" algorithm (60 s for the measurement: 30 s for each energy range): Cu = 86.6 ± 0.5 wt%, Sn = 11.9 ± 0.4 wt%, Pb = 0.97 ± 0.1 wt%, Ni = 0.2 ± 0.02 wt%, Zn = 0.19 ± 0.04 wt%, Sb = 0.09 ± 0.02 wt%.

XRF analyses of two copper-alloyed toilet spoons from the Museo Egizio were carried out by using the "Patina" algorithm (120 s) and the "Metals" algorithm (60 s) and the 3 mm spot analysis configuration.

Diffraction was carried out using a X'Pert PRO PW3050/60 PANalytical instrument equipped with a fast curved 1D silicon strip de-tector (X'celerator) operating at 40 kV and 30 mA with a Cu Kα radia-tion. The patterns analysis was obtained using a Bruker proprietary software (DIFFRACplus) and the Powder Diffraction File (PDF) database of The International Centre for Diffraction Data (ICDD). The patinas were analysed without any preparation (to preserve them) by inserting the specimens directly into the diffractometer.

Afterwards, the samples were sliced transversely, they were embed-ded in epoxy resin SpeciFix-40 (STUERS ApS – Denmark) and then polished for observation under a LEICA 2500 M metallographic micro-scope equipped with an N PLAN (achromatic objectives up to 1000×) and LEICA DFC295 digital camera at 5 M pixels, and polarization crystals. Observations were made of the sample surface, to detect the presence of corrosion products, and of the cross-section, to observe the stratigraphy of the corrosion patina and to measure its thickness. The corrosion prod-ucts were characterised by a metallographic microscope with a dark field (DF) contrast system.

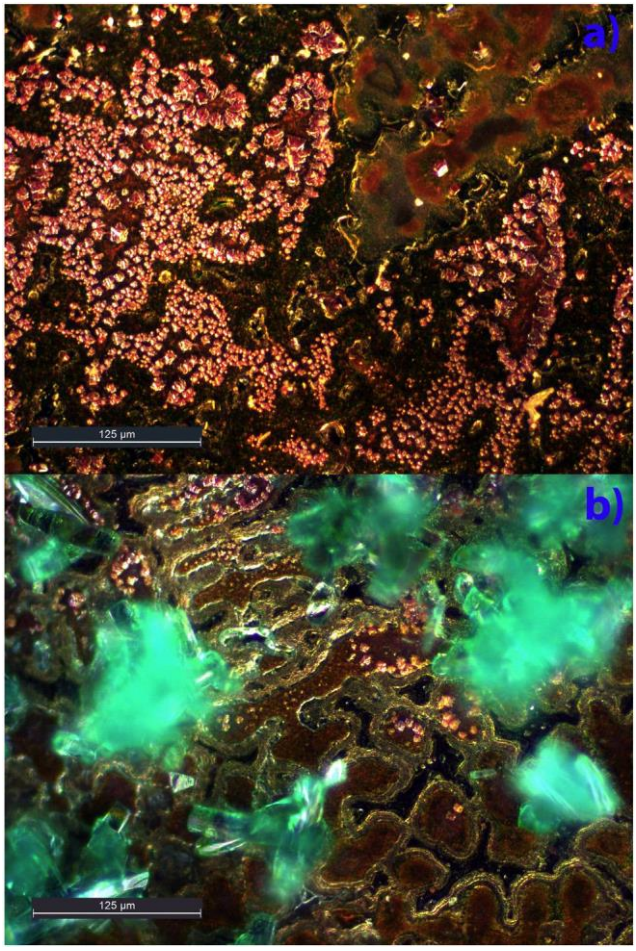

Fig. 3. Metallographic microscope micrographs of the bronze surface covered by cuprate crystals after 1 day (a), and brochantite green crystals developed above the red layer after 10 days (b). (For interpretation of the references to colour in this figure legend, the reader is referred to the web version of this article.)

The samples were observed by Scanning Electron Microscopy using a JEOL JSM-IT300LV with Energy dispersion spectrometer Oxford INCA Energy 200 and PENTAFET detector (SATW). The working conditions

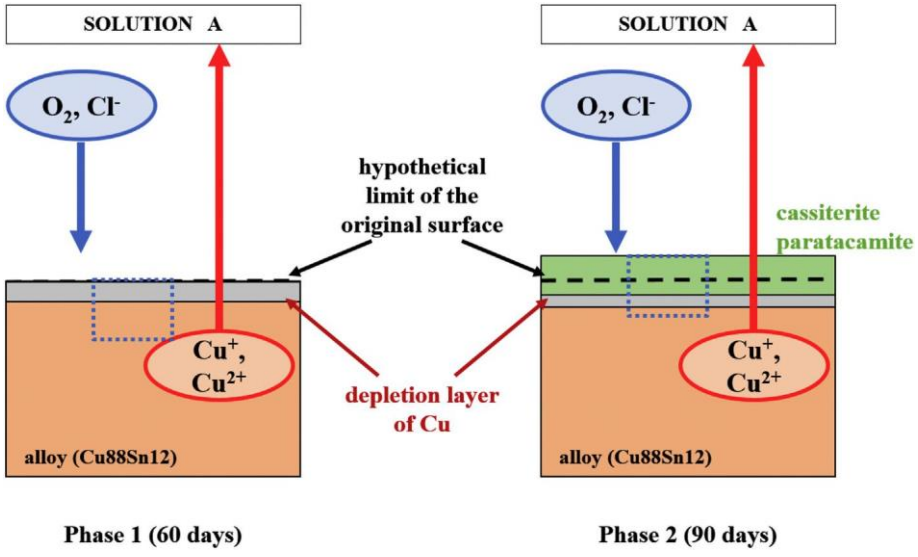

Fig. 2. Schematic representation of the corrosion layers developed in the solution A during 90 days of immersion. The blue rectangle is the volume analysed by pXRF spectrometer. (For interpretation of the references to colour in this figure legend, the reader is referred to the web version of this article.)

Table 1

Average thickness of the corrosion products of the CuSn12 samples immersed in solution B, measured in cross-section using the metallograhic microscope.

Degree of corrosion	1	2	3	4	5	6	7	8	9
Red layer (μm)	1.1	7.6	6.8	6.2	2.9	2.7	6.4	4.6	2.1
Green crystals layer (μm)	–	–	–	6.4	19.1	36.9	49.4	81.8	98.1

were 15.0 kV and 300 pA and line analysis was carried out to determine that the cross section composition was recorded for 256 measuring points. The specimens embedded in epoxy resin were also polished on the back of the samples to guarantee electric conduction during the EDS measurements. SEM observations were made using both a back-scatter (BED-C) and secondary electron (SED) detector.

3. Results and discussion

Initially, the portable instrumentation was calibrated by using CRM. Calibration was carried out by using different algorithms and focusing on the evaluation of analytical accuracy (more details are reported as supplementary information in Appendix A).

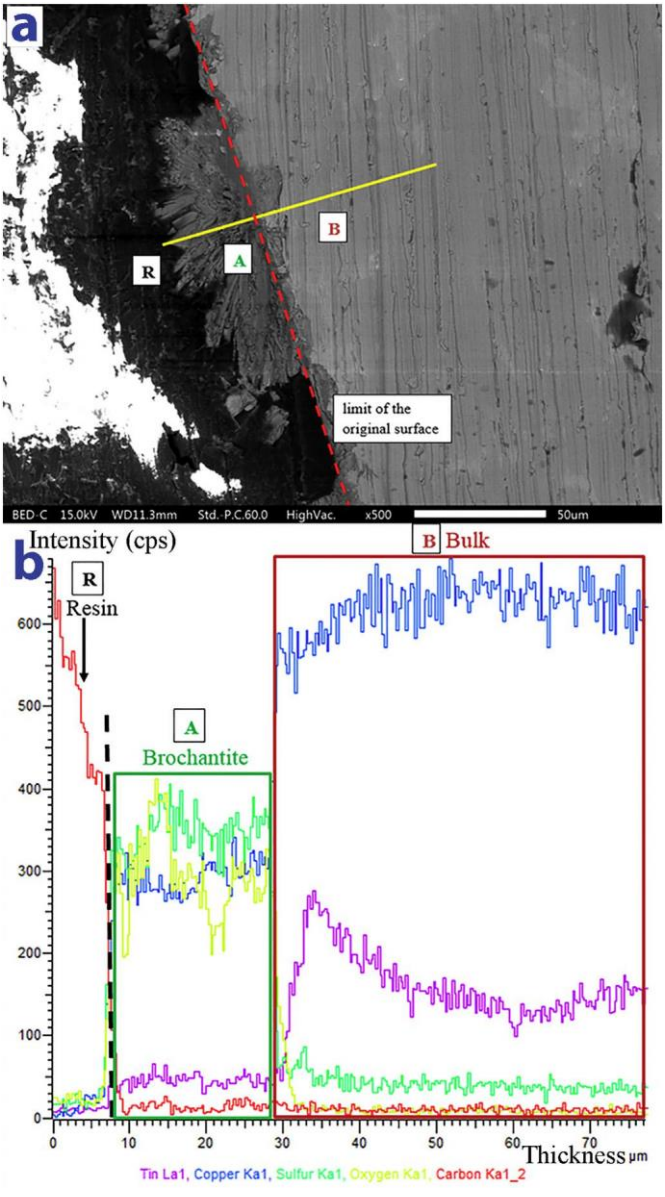

Fig. 4. SEM micrograph (a) and EDS diagram (b) of B_90d with the indication of patinas evolution.

3.1. Solution A

In the samples treated with the ammonium carbonate and ammo-nium chloride solution, the alteration observed at the surface was not significant up to 30 days. Only after 60 days there was a uniform light blue patinated layer detected by the metallographic microscope (XRD patterns are reported in Appendix A, figures S4_1).

The cross section SEM-EDS analysis carried out on the corrosion pa-tina of sample A_90d revealed the presence of a tin reach corrosion layer that may support the hypothesis of the development of chloride or oxide Sn corrosion products that appears to be detached and fragmented due to the cross cutting and subsequent polishing of the samples. At the corrosion layer/bulk interface, EDS analysis revealed the presence of Cu, Sn and Cl, which was probably linked to a mixture of Cu chlorides and Sn oxides or chlorides (Fig.1). After 90 days, the thickness of the corrosion products was about 200 μm, including voids and not homogeneous areas.

The XRD analysis, performed on the sample A_90d, confirms the presence of cassiterite (SnO_2) and paratacamite ($Cu_2(OH)_3Cl$) probably besides other amorphous corrosion products of Cu and Sn.

The Cu and Sn concentrations, determined by XRF analysis, up to 30 days, lay within the error bar of the initial measured composition, confirming the metallographic microscope observations and SEM-EDS analyses, where no remarkable morphological and composi-tional variations were observed. Moreover, between 60 days and 90 days, the Cu concentration determined by the XRF “Metals” algorithm decreased from 78 wt% to 48 wt% and the Sn concentration increased up to 43.3 wt% in A_90d. The normalisation of the XRF data obtained with the “Patina” algorithm leading to Cu and Sn concentra-tions with values close to those obtained using the “Metals” algorithm (the complete data are reported in table S1 in Appendix A).

The corrosion model acting for samples immersed in solution A is depicted in Fig. 2. It initially involves the development of a Cu depletion layer at the surface of the sample due to decupri-fication without the de-velopment of corrosion products up to 60 day of immersion in the corro-sive solution (Phase 1). Subsequently, we can assume the development of Sn corrosion products (tin oxides or tin chlorides) and copper chloride corrosion products in A_90d (Phase 2). XRD analysis confirms the pres-ence of tin oxide cassiterite and copper hydroxychloride paratacamite. In solution A, the XRF data become less accurate after 60 days due to

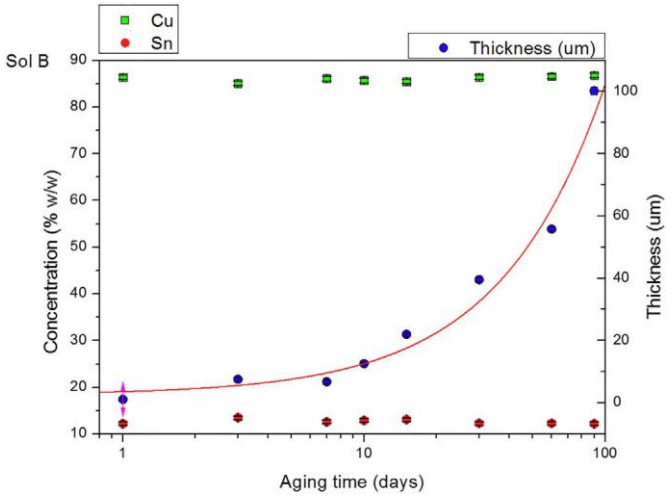

Fig. 5. Cu and Sn concentration vs aging time in solution B correlated with the increasing of corrosion layer thickness. The red curve indicates the linear regression of the patina growth. (For interpretation of the references to colour in this figure legend, the reader is referred to the web version of this article.)

Table 2
Average thickness of the corrosion products of the CuSn12 samples immersed in solution C, measured in cross-section using the metallograhic microscope.

Degree of corrosion	1	2	3	4	5	6	7	8	9
Green layer (μm)	47.6	36.7	47.7	35.1	41	56.8	98.5	115	150

the depletion of Cu that produces a rich Sn surface layer that leads to an increase in the Sn concentration. After 90 days, the composition measured by XRF is limited to the depletion layer and the corrosion products, due to their thickness that is higher than the volume interaction of the XRF. Therefore, the Cu concentration decreases strongly in A_90d due to the growth of the Sn corrosion layer and to the Cu depletion layer at the same time (Fig. 2).

3.2. Solution B

The second solution chosen is a mixture of potassium chloride, cu-pric sulphate pentahydrate and sodium sulphate decahydrate, which is more aggressive because of the addition of sulphuric acid to obtain a pH = 3.

The metallographic microscope observations show the development of red crystals just after 1 day (Fig. 3a), that grow up to form a uniform layer in B_7d.

From 10 days some green crystals develop above the red layer (Fig.3b). The red layer has a variable thickness from 1 μm to 7.6 μm. The green crystals have an increasing thickness up to about 100 μm in B_90d (Table 1).

The XRD analysis performed on B_60d allows to clearly identify red crystals as cuprite (Cu_2O) and green crystals as brochantite ($Cu_4SO_4(OH)_6$) due to the corrosion process (XRD patterns are reported in Ap-pendix A, figures S4_2).

The SEM-EDS analyses of samples from B_15d to B_90d confirm the presence of copper sulphate. The analysis on the brocanthite crystals identifies the elements Cu, S and O (Fig.4b). The limit of the original sur-face is preserved (Fig.4a).

The Cu apparent concentration, obtained with the "Patina" algo-rithm decreases from 86.6 wt% (initial measured concentration) to 66.2 wt% after 90 days of immersion. The Sn/Cu ratio does not change from B_1d to B_90d and the Sn concentration is equal to the initially measured composition in B_90d (12.2 wt%) using the "Metals" algo-rithm. In addition, the "Patina" algorithm detects no appreciable change in the Sn concentration (the complete data are reported in table S3_1 in Appendix A). The development of the crystals of cuprite and brochantite (maximum 100 μm in thickness) has no effect on the XRF measure-ments (Fig.5).

3.3. Solution C

Macroscopically, a powdery thin green layer covers the specimens at each immersion time. The thickness of this patina varies from 35 μm (C_10d) to 150 μm in C_90d (Table 2).

The XRD analysis of the sample C_60d identifies atacamite and paratacamite phases. The presence of atacamite and paratacamite indi-cates a well-known bronze disease [31–34] which disrupts the surface and can disfigure the artefact [35]. The corrosion layer has a globular structure and the corrosion products have strongly penetrated into the metallic bulk of the alloy.

The SEM-EDS analyses of the samples from C_30d to C_90d detect a corrosion product of Cu and Cl above Sn\\Cl corrosion products (Fig.6a and b). Probably, the latter develops before 30 days of immersion. This

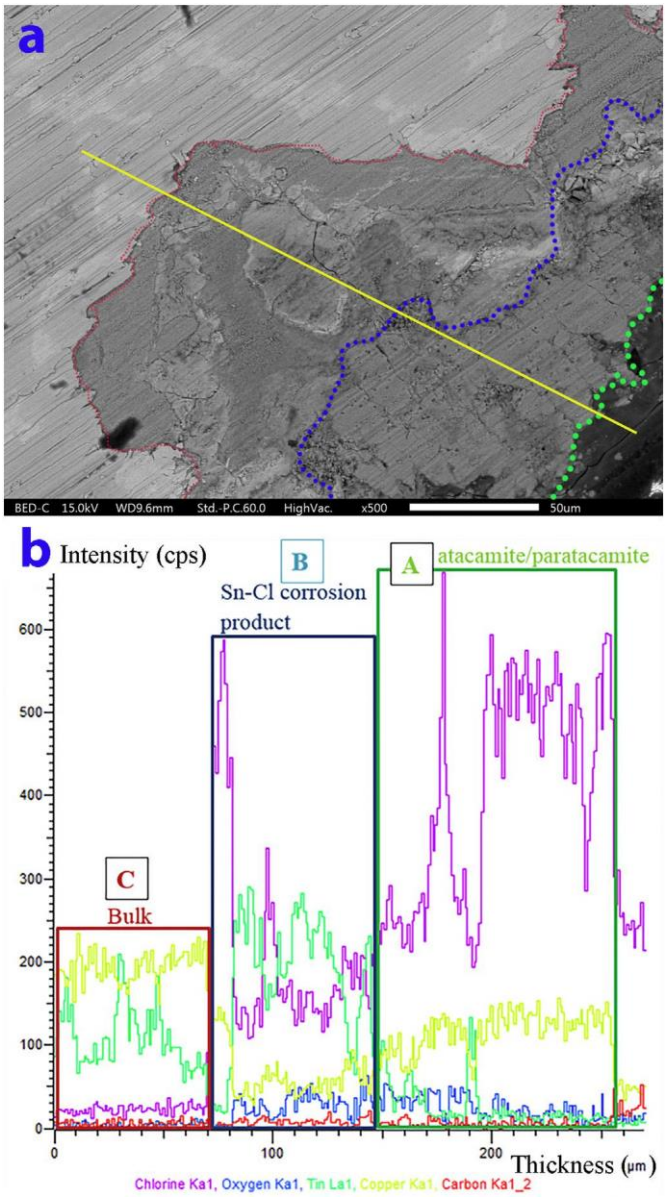

Fig. 6. SEM micrograph (a) and EDS diagram (b) of the sample C_90d with the indication of patinas evolution.

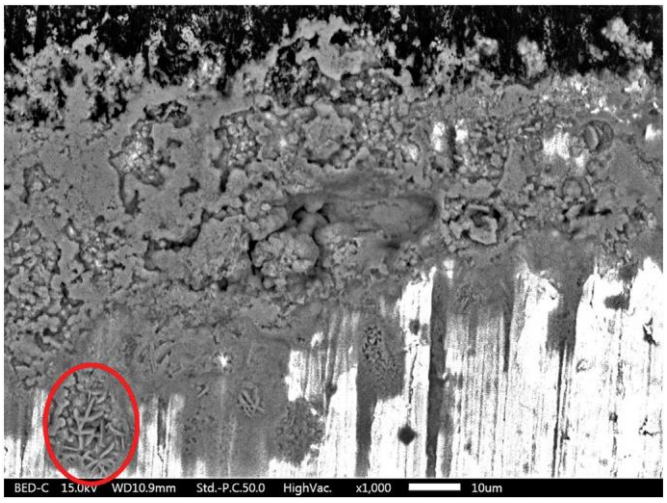

Fig. 7. Cross-section micrograph of the corrosion layers of the sample C_30d. Red circled area probably shows needles of romarchite (SnO). (For interpretation of the references to colour in this figure legend, the reader is referred to the web version of this article.)

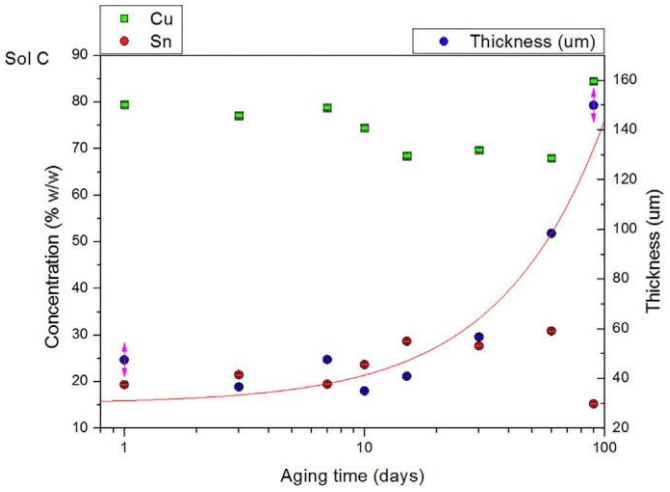

Fig. 8. Cu and Sn concentration vs aging time in solution C correlated with the increasing of corrosion layer thickness. The red curve indicates the linear regression of the patina growth. (For interpretation of the references to colour in this figure legend, the reader is referred to the web version of this article.)

corrosion product is not identified by XRD analysis due to the thickness of the overlying atacamite/paratacamite layer in C_60d.

The results of the XRF measurements with the normalized "Patina" algorithm show that the Cu concentration constantly decreases from C_1d (78 wt%) to C_60d. (67 wt%). The Sn concentration grows steadily up to C_60d (32 wt%), then decreases after 80 days (7 wt%) and it be-comes equal to 16 wt% in C_90d. The Pb concentration ranges from 0.3 wt% to 0.9 wt% up to C_60d and after 90 days it becomes equal to 0.05 wt%. The Cl concentration detected with the "Patina" algorithm in-creases up to C_10d and is stabilised around 10 wt%. The XRF measure-ments performed with the "Metals" algorithm after 90 days detect the Cu and Sn concentrations close to the initial measured composition (Cu = 84.5 ± 0.04 wt%; Sn = 15.3 ± 0.05 wt%).

XRF data obtained with the "Patina" algorithm show the evolution of the corrosion process (the complete data are reported in table S3_2 in Appendix A). In C_1d the selective dissolution of Cu leads to a conse-quent increasing of the Sn concentration (decuprification) in the sur-face layer accompanied by the presence of mixed Cu and Sn and Sn oxides identified in other studies as cuprite (Cu_2O) romarchite (SnO), cassiterite (SnO_2) and/or oxyhydroxide as hydroromarchite ($5SnO{\cdot}2H_2O$) [36–38]. Decuprification and the development of Sn species (oxides, chlorides) are in agreement with the Type I patina of ancient bronzes. The SEM micrograph in Fig.7 shows the same needle morphology of crystals identified by Dunkle on pewter as romarchite (SnO).

From C_3d copper chlorides are developed, probably cuprous chloride CuCl (nantokite) in accordance with the increase in the Cl concentration (10 wt%) [39,40], that implicates heavy inter-granular corrosion phenom-ena by chlorine and the embrittlement of the artefact [41]. Subsequently, it develops a layer of atacamite and paratacamite as highlighted by XRD analysis in sample C_60d (XRD patterns are reported in Appendix A, figures S4_3). The same morphology of the corrosion patina is observed

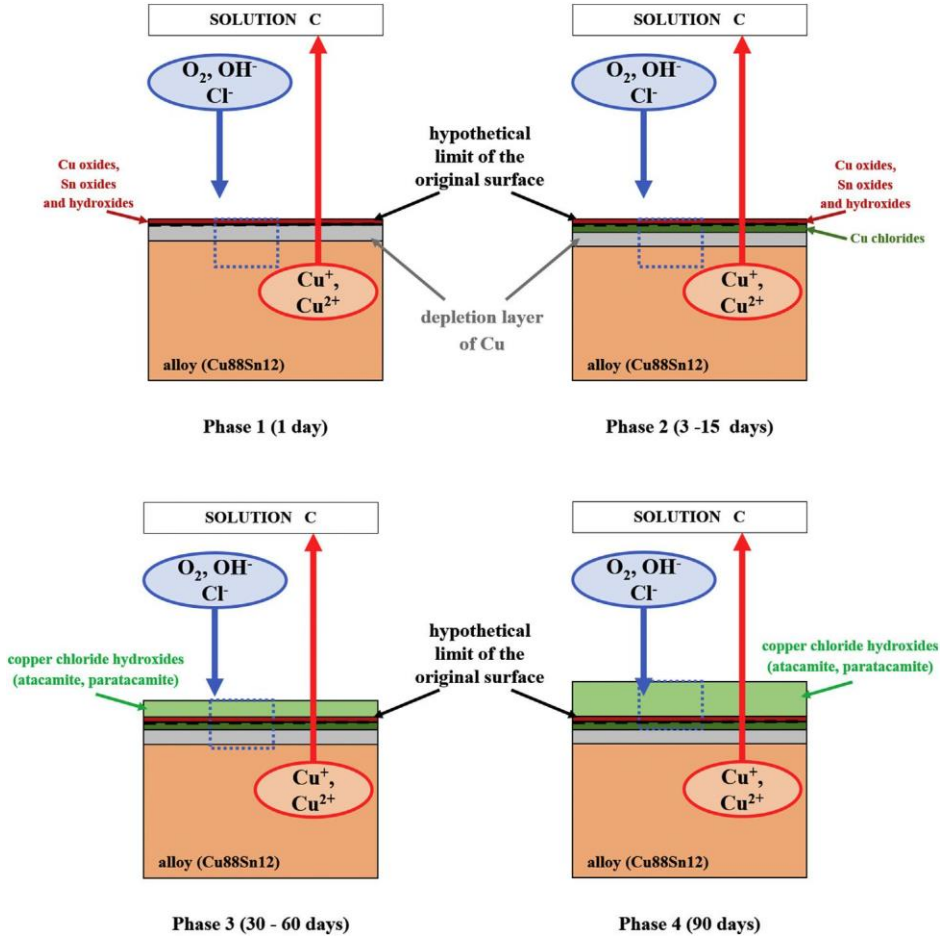

Fig. 9. Schematic representation of the corrosion layers developed in solution C during 90 days of immersion. The blue rectangle is the volume analysed by pXRF spectrometer. (For interpretation of the references to colour in this figure legend, the reader is referred to the web version of this article.)

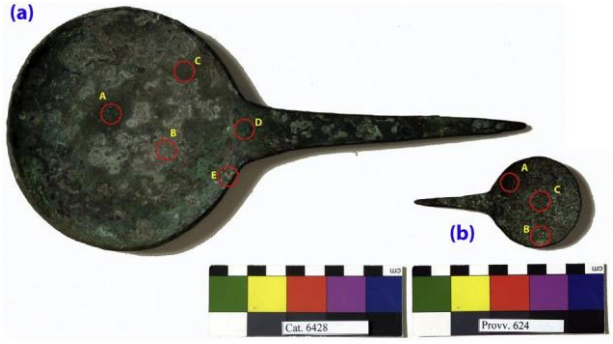

Fig. 10. Frontside of the two Egyptian toilet spoons C.6428 (a) and P.624 (b) with points of analysis.

after 30 days of immersion. Cuprous chloride develops a pH = 3.5–4.0 and from its oxidation and hydrolysis, the copper trihydroxychlorides take place according to the following reaction [31]:

$$4CuCl + O_2 + 4H_2O \leftrightarrow 2Cu_2(OH)_3Cl + H^+ + Cl^-$$

Cross section SEM-EDS analyses on C_60d, and C_90d show an inner layer of Sn chloride species that can be developed previously, between 3 and 15 days of immersion because the Sn concentration continues to in-crease steadily. The chlorination of Sn(II)/Sn(IV) oxyhydroxide species leads to the formation of Sn chloride oxyhydroxide as abhurite ($Sn_{21}Cl_{16}(OH)_{14}O_6$). Sn chloride oxyhydroxide species were detected on the corrosion patina of the $Cu_{90}Sn_{10}$ alloy exposed in NaCl 0.1 M aqueous solution (pH 6.5) in thermodynamic equilibrium with air at room temperature [42]. Around 90 days, the XRF data become more affected by the corrosion layers and, therefore, the measured alloy com-position is less and less consistent with the original alloy composition (Fig. 8):

the Cu concentration increases with the thickness of corrosion layers; at the same time the Sn concentration decreases greatly, probably because the volume analysed by the XRF spectrometer does not cross the inner layer of the Sn chloride species. Conse-quently, in C_90d, the XRF spectrometer does not detect the Sn concentration of the bulk, but only the Sn-Cl corrosion products (Fig. 9).

3.4. Elemental composition of copper-alloyed Egyptian artefacts

The second part of this study concerns the in situ XRF measure-ments of Egyptian copper tin alloys with similar composition of corroded bronze samples used in laboratory experiments, as discussed previously.

At the beginning of the last century, the toilet spoon C.6428 was classified by Bénédite as an Egyptian bronze mirror with a concave disk and a slight depression 1 mm thick at the centre [43]. The artefact P.624 is a model of the toilet spoon characterised by the small size.

XRF measurements were made in different points (Fig. 10) in order to obtain statistical information on the detection of chemical composi-tion of bronze alloys. The results show that the toilet spoons are bronzes containing lead impurities.

As the results of the accelerated corrosion of samples C have demonstrated, the green patinas with a high concentration of chlorine (8–11 wt%) observed in extended areas on the toilet spoon C.6428, could be atacamite and/or paratacamite. The grey patina of the same spoon, by contrast, is characterised by high levels of sulphur (10 wt%) and the red patina probably is constituted by cuprous oxide (cuprite). The apparent concentration of copper is lower in the point of analysis
D (54 wt%) than other points (62.9–67.3 wt%). In the toilet spoon C.6428, the tin concentration is lower on the green and dark green patinas, (with values between 4.3 wt% and 5.4 wt%) than grey and red patinas (11.3–12.6 wt%).

The green patina has an extensive presence and a uniform colour on the toilet spoon P.624. The concentration of sulphur is higher in measuring point B (7 wt%) than other measuring points (4–5 wt%). Point C shows similar concentrations of chlorine and sulphur. Tin concentration of toilet spoon P.624 is very similar in all measured points (11.2–12.8 wt% with the normalized “Patina” algorithm; 10.1–11.4 wt% using the “Metals” algorithm).

In correspondence to the green and dark green patinas of the spoon C.6428, low Sn concentrations were detected with respect to the red and grey patinas. This result can be explained with the decrease in Sn concentration due to the thickness and density of green corrosion pati-nas that can exceed the penetration depth of the XRF analysis. Indeed, it is well known that the copper chloride species can develop above the cuprite layer and consequently the green patinas have a greater thick-ness that the other patinas. The grey-green patinas of the spoon P.624 showed similar Sn concentration, suggesting low thickness of the corro-sion layers.

As can be seen from Tables 3 and 4, the concentrations of the alloying elements measured with both algorithms are comparable and lay within the error bar. It is possible to obtain the average chemical compositions of the two toilet spoons by subtracting the chemical concentrations of soil and patina elements (e.g. Ca, Si, Al, K, P, Cl, S) and after appropriate normalisation of the alloying element concentra-tions. The average composition of the toilet spoon C.6428 without atten-uation effects (points of analysis B and E with the normalized “Patina” algorithm and with the “Metals” algorithm) is Cu = 85.1 ± 1.2 wt%, Sn = 14.8 ± 1.2 wt%, Pb = 0.13 ± 0.04 wt%. The average composition

Table 3
Results of the chemical composition using the “Patina” algorithm of the toilet spoons C.6428 and P.624 from the Museo Egizio (Turin). The chemical concentration is expressed in weigh percentage (wt%). Note: $Cu_{(N)}$, $Sn_{(N)}$ and $Pb_{(N)}$ are the normalized concentrations of the alloying elements; SD = standard deviation.

Artefact ID	Measuring point	Patina	Cu	$Cu_{(N)}$	Sn	$Sn_{(N)}$	Pb	$Pb_{(N)}$	Fe	Cl	S	Ca	Si	K
C.6428	A	Green	67.3	93.6	4.6	6.3	0.02	0.03	0.07	7.8	2.6	0.7	1.1	0.1
	B	Grey	64.7	85.1	11.3	14.8	0.06	0.08	0.27	1.1	10.0	1.2	0.9	0.3
	C	Green	62.9	91.9	5.4	8.0	0.08	0.12	0.09	10.5	3.6	0.9	1.4	0.1
	D	Dark green	54.0	92.6	4.3	7.3	0.05	0.08	0.06	9.3	4.9	0.6	0.5	0.2
	E	Red	64.6	83.6	12.6	16.3	0.10	0.13	0.30	5.7	2.7	1.3	1.1	0.2
	Mean			89.3		10.6		0.10						
	SD			4.7		4.6		0.04						
P.624	A	Dark green	65.0	87.9	8.3	11.2	0.56	0.76	0.69	5.4	3.6	2.7	3.5	0.3
	B	Green	58.4	86.5	8.6	12.8	0.44	0.65	0.36	4.4	7.2	2.6	2.1	0.1
	C	Green	55.4	86.9	7.9	12.4	0.43	0.67	0.26	4.4	4.7	1.7	1.8	0.1
	Mean			87.1		12.2		0.70						
	SD			0.7		0.8		0.06						

Table 4
Results of the chemical composition using the "Patina" algorithm of the toilet spoons C.6428 and P.624 from the Museo Egizio (Turin). The chemical concentration is expressed in weigh percentage (wt%). Note: $Cu_{(N)}$, $Sn_{(N)}$ and $Pb_{(N)}$ are the normalized concentrations of the alloying elements; SD = Standard Deviation; Error = algorithm error.

Artefact ID	Measuring point	Patina	Cu	Error (±)	Sn	Error (±)	Pb	Error (±)
C.6428	A	Green	94.2	0.1	5.78	0.07	0.04	0.01
	B	Grey	86.6	0.1	13.33	0.08	0.12	0.02
	C	Green	92.3	0.1	7.59	0.06	0.17	0.02
	D	Dark green	92.5	0.1	7.38	0.07	0.14	0.02
	E	Red	85.2	0.1	14.64	0.08	0.17	0.02
	Mean		90.1		9.74		0.13	
	SD		4.0		3.96		0.05	
P.624	A	Dark green	88.7	0.1	10.14	0.07	1.12	0.04
	B	Green	86.7	0.1	12.45	0.09	0.90	0.05
	C	Green	87.7	0.1	11.41	0.08	0.93	0.04
	Mean		87.7		11.33		0.98	
	SD		1.0		1.16		0.12	

of the toilet spoon P.624 is Cu = 87.4 ± 0.9 wt%, Sn = 11.7 ± 1.0 wt%, Pb = 0.8 ± 0.2 wt%, considering all points of analysis carried out with both algorithms.

4. Conclusions

The study of the degradation phenomena of $Cu_{88}Sn_{12}$ corroded samples allowed the changing and reliability of the composition analysis detected by X-ray Fluorescence Spectroscopy to be observed.

XRF measurements on the accelerated corrosion samples made it possible to obtain information about instrumental accuracy in the de-tection of the chemical composition of metallic bulk. The initial chemical concentrations of the alloying elements up to a thickness of the corro-sion patina of about 100 μm were measured on samples exposed to solution B. In solution C, the development of copper chloride and hydroxychloride patinas with high thickness prevented the correct evaluation of the alloying elements.

The combined use of both the "Patina" and "Metals" algorithms made it possible to obtain information about the evolution of corrosion processes (e.g. decuprification and development of Sn corrosion prod-ucts in samples A and C) and the composition of the patinas.

Furthermore, handheld XRF allowed the in situ chemical characteri-sation of two Egyptian toilet spoon C.6428 and P.624 with an amount of tin between about 12 and 15 wt%. The most reliable XRF data were mea-sured on red and grey corrosion patinas.

The accuracy of the XRF data is obtained by analysing many points and comparing the chemical composition of different corrosion patinas to achieve statistical information of the alloy bulk.

In conclusion, this work made it possible to establish on which cor-rosion patinas pXRF can detect concentrations of the alloying elements with greater accuracy.

Acknowledgements

The authors would like to thank the team of the Museo Egizio (Turin), in particular Sara Aicardi, for collaboration in the study of the Egyptian bronze artefacts. We acknowledge the Soprintendenza Archeologia, Belle Arti e Paesaggio per la città metropolitana di Torino, for providing archaeological information of the Egyptian bronzes. The authors are grateful to Elettra Fabbri (Department of Engineering, Uni-versity of Ferrara) for her collaborations, Gaia Fenoglio (Department of Chemistry, University of Turin), Maurizio Aceto (Dipartimento di Scienze e Innovazione Tecnologica (DISIT), Università degli Studi del Piemonte Orientale) and Giulia Penaglia to the help during the chemical analyses of the Egyptian artefacts.

References

[1] G. Vittiglio, K. Janssens, B. Vekemans, F. Adams, A. Oost, A compact small-beam XRF instrument for in-situ analysis of objects of historical and/or artistic value, Spectrochim. Acta B 54 (1999) 1697–1710.
[2] S. Shalev, S.S. Shilstein, Y. Yekutieli, XRF study of archaeological and metallurgical material from an ancient copper-smelting site near Ein-Yahav, Israel, Talanta 70 (2006) 909–913.
[3] T. Čechák, M. Hložek, L. Musílek, T. Trojek, X-ray fluorescence in investigations of archaeological finds, Nucl. Inst. Methods Phys. Res. B 263 (2007) 54–57.
[4] A. Vasilescu, B. Constantinescu, XRF-based compositional microanalysis for prove-nance studies of metallic artifacts, Romanian Rep. Phys. 63 (4) (2011) 901–911.
[5] S. Ridolfi, Portable X-ray fluorescence spectrometry for the analyses of cultural her-itage, IOP Conf. series: materials science and engineering, International Conference on the Use of X-ray (and Related) Techniques in Arts and Cultural Heritage (XTACH 11)vol. 37, 2012, p. 012001.
[6] M. Ferretti, The investigation of ancient metal artefacts by portable X-ray fluores-cence devices, J. Anal. At. Spectrom. 29 (2014) 1753–1766.
[7] D. Šatović, V. Desnica, S. Fazinić, Use of portable X-ray fluorescence instrument for bulk alloy analysis on low corroded indoor bronzes, Spectrochim. Acta B 89 (2013) 7–13.
[8] R. Fernandes, B.J.H. van Os, H.D.J. Huisman, The use of Hand-Held XRF for investigating the composition and corrosion of Roman copper-alloyed artefacts, Herit. Sci. 1 (1) (2013).
[9] E. Angelini, A. Batmaz, A. Çilingiroğlu, S. Grassini, G.M. Ingo, C. Riccucci, Tailored analytical strategies for the investigation of metallic artefacts from the Ayanis Fortress in Turkey, Surf. Interface Anal. 42 (6–7) (2010) 675–679.
[10] M.F. Alberghina, R. Barraco, M. Brai, T. Schillaci, L. Tranchina, Integrated analytical methodologies for the study of corrosion processes in archaeological bronzes, Spectrochim. Acta B 66 (2011) 129–137.
[11] F. Faraldi, A. Çilingiroğlu, E. Angelini, C. Riccucci, T. De Caro, A. Batmaz, A. Mezzi, D. Caschera, B. Cortese, Micro-chemical and micro-structural investigation of archaeological bronze weapons from the Ayanis fortress (lake Van, Eastern Anatolia, Tur-key), Appl. Phys. A 113 (2013) 911–921.
[12] L. Robbiola, J.M. Blengino, C. Fiaud, Morphology and mechanisms of formation of natural patinas on archaeological Cu-Sn alloys, Corros. Sci. 40 (12) (1998) 2083–2111.
[13] C. Soffritti, E. Fabbri, M. Merlin, G.L. Garagnani, C. Monticelli, On the degradation factors of an archaeological bronze bowlbelonging to a private collection, Appl. Surf. Sci. 313 (2014) 762–770.
[14] G. Brunton, G. Caton-Thompson, The Badarian civilisation and predynastic remains near Badari, British School of Archaeology in Egypt, London, 1928.
[15] H.C.H. Carpenter, An Egyptian axe head of great antiquity, Nature 130 (1932) 625–626.
[16] A. Lucas, J.R. Harris, Ancient Egyptian Materials and Industries, fourth ed. Arnord, London, 1962.
[17] J. Riederer, Die naturwissenschaftliche Untersuchung der Bronzen des Ägyptischen Museums Preußischer Kulturbesitz in Berlin, Berl. Beitr. Archaeom. 3 (1978) 5–42.
[18] J. Riederer, Metal analysis of Egyptian bronzes, Revue d'Archaeometrie 3 (1981) 239–243.
[19] J. Riederer, Die naturwissenschaftliche Untersuchung der Staatlichen Sammlung Ägyptischer Kunst in München, Berl. Beitr. Archaeom. 7 (1982) 5–34.
[20] J. Riederer, Metallanalysen ägyptischen Statuetten des Kestner-Museums, Berl. Beitr. Archaeom. 8 (1983) 5–17.
[21] J. Riederer, Die naturwissenschaftliche Untersuchung der Ägyptischen Bronzen des Pelizaeus-Museums in Hildesheim, Berl. Beitr. Archaeom. 9 (1984) 5–16.
[22] J. Riederer, Metallanalysen ägyptischen Bronzestatuetten aus Deutschen Museen, Berl. Beitr. Archaeom. 10 (1988) 5–20.
[23] E.R. Eaton, H. McKerrell, Near eastern alloying and some textual evidence for the early use of arsenical copper, World Archaeol. 8 (2) (1976) 169–191.
[24] R.M. Cowell, Scientific appendix I: chemical analyses, in: W.V. Davies (Ed.), Cata-logue of Egyptian Antiquities in the British Museum. VII, Tools and Weapons. I, Axes, British Museum Publications, London 1987, pp. 96–118.
[25] J. Ogden, Metals, in: P.T. Nicholson, I. Shaw (Eds.), Ancient Egyptian Materials and Technology, Cambridge University Press, Cambridge 2000, pp. 148–176.

[26] S.J. Fleming, J. Crowfoot-Payne, PIXE analyses of some Egyptian bronzes of the Late Period, MASCA, Journal 1 (2) (1979) 46–47.
[27] V. Hayez, V. Costa, J. Guillaume, H. Terryn, A. Hubin, Micro Raman spectroscopy used for the study of corrosion products on copper alloys: study of the chemical compo-sition of artificial patinas used for restoration purposes, Analyst 130 (2005) 550–556.
[28] K. Leyssens, A. Adriaens, C. Degrigny, E. Pantos, Evaluation of corrosion potential measurements as a means to monitor the storage and stabilization processes of ar-chaeological copper-based artifacts, Anal. Chem. 78 (8) (2006) 2794–2801.
[29] M. Ghoniem, The characterization of a corroded Egyptian bronze statue and a study of the degradation phenomena, In. J. Conserv. Sci. 2 (2) (2011) 95–108.
[30] V.K. Gouda, G.I. Youssef, N.A. Abdel Ghany, Characterization of Egyptian bronze ar-chaeological artifacts, Surf. Interface Anal. 44 (2012) 1338–1345.
[31] D.A. Scott, Bronze disease: a review of some chemical problems and the role of rel-ative humidity, J. Am. Inst. Conserv. 29 (1990) 193–206.
[32] D.A. Scott, A review of copper chlorides and related salts in bronze corrosion and as painting pigments, Stud. Conserv. 45 (1) (2000) 39–53.
[33] A. Mezzi, E. Angelini, C. Riccucci, S. Grassini, T. De Caro, F. Faraldi, P. Bernardini, Micro structural and micro-chemical composition of bronze artefacts from Tharros (Western Sardinia, Italy), Surf. Interface Anal. 44 (2012) 958–962.
[34] R. Grayburn, M. Dowsett, M. Hand, P.J. Sabbe, P. Thompson, A. Adriaens, Tracking the progression of bronze disease – a synchrotron X-ray diffraction study of nantokite hydrolysis, Corros. Sci. 91 (2015) 220–223.
[35] M.P. Casaletto, T. De Caro, G.M. Ingo, C. Riccucci, Production of reference “ancient” Cu-based alloys and their accelerated degradation methods, Appl. Phys. A 83 (2006) 617–622.
[36] S.E. Dunkle, J.R. Craig, J.D. Rimstidt, W.R. Lusardi, Romarchite, hydroromarchite and abhurite formed during the corrosion of pewter artifacts from the Queen Anne's re-venge (1718), Can. Mineral. 41 (2003) 659–669.
[37] S.E. Dunkle, J.R. Craig, W.R. Lusardi, Romarchite and associated phases as common corrosion products on pewter artifacts from marine archaeological sites, Geoarchaeology 19 (6) (2004) 531–552.
[38] C. Riccucci, G.M. Ingo, A. Faustoferri, M.I. Pierigè, E.I. Parisi, G. Di Carlo, T. De Caro, F. Faraldi, Micro-chemical and metallurgical study of Samnite bronze belts from an-cient Abruzzo (central Italy, VIII–IV BC), Appl. Phys. A 113 (2013) 959–970.
[39] J. Wang, C. Xu, G. Lv, Formation processes of CuCl and regenerated Cu crystals on bronze surfaces in neutral and acidic media, Appl. Surf. Sci. 252 (2006) 6294–6303.
[40] X. Zhang, I.O. Wallinder, C. Leygraf, Mechanistic studies of corrosion product flaking on copper and copper-based alloys in marine environments, Corros. Sci. 85 (2014) 15–25.
[41] G.M. Ingo, A. Çilingiroğlu, F. Faraldi, C. Riccucci, M.P. Casaletto, A. Erdem, A. Batmaz, The bronze shields found at the Ayanis fortress (Van region, Turkey): manufacturing techniques and corrosion phenomena, Appl. Phys. A 100 (2010) 793–800.
[42] L. Robbiola, T.T.M. Tran, P. Dubot, O. Majerus, K. Rahmouni, Characterisation of an-odic layers on Cu–10Sn bronze (RDE) in aerated NaCl solution, Corros. Sci. 50 (2008) 2205–2215.
[43] M.G. Bénédite, Catalogue Générale des Antiquités Égyptiennes du Musée du Caire. N^{os} 44001-44102. Miroirs, Imprimerie de l'Institut Français d'Archéologie Orientale, 1907.